Studies of the Crab Nebula based upon 400 hours of Observations with the HEGRA System of Cherenkov Telescopes

D. Horns (*dieter.horns@mpi-hd.mpg.de*), for the HEGRA collaboration
MPI f. Kernphysik, Postfach 10 39 80, D-69117 Heidelberg, Germany

Abstract

The Crab nebula has been observed extensively with the HEGRA system of imaging air Cherenkov telescopes. Roughly 400 hours of prime observation time at zenith angles between 5 and 65 degrees have been dedicated to the standard candle in TeV astronomy. Based upon the data set gathered during the 5 years of operation of the HEGRA telescopes, the energy spectrum has been reconstructed. The energy spectrum extends from 500 GeV beyond 20 TeV and allows to constrain the position of a possible high-energy cut-off.

1. Introduction

The Crab nebula has been a prime target of observations since the beginning of operation of the instrument primarily for calibration and monitoring of the instrument's γ-efficiency in the initial stage of operation and during the routine operation. The observational results include the energy spectrum [3], upper limits on the angular size of the emitting region [4], and constraints on the fraction of pulsed radiation [5]. After the end of the live-time of the instrument (it has been dismantled in October 2002), an analysis of the entire dataset taken from the Crab nebula with increased statistics and improved reconstruction technique with respect to previous publications [2] (the most recent published spectrum from the Crab nebula is based upon $\approx$ 150 hrs of observations) is justified and first preliminary results on the energy spectrum are presented here.

2. Observations and Results

The observations had been carried out between September 1997 and September 2002. During it's life-time as a 4 (later 5) telescope system, the setup of the individual telescopes (including cameras and electronics) has not been modified. However, the degradation of the mirrors and the ageing of the photomultipliers have been compensated by an increase of the high voltage on an annual basis. The performance of the instrument has been closely monitored by various checks on the acceptance, absolute calibration with muon-rings, cut efficiencies, pointing calibration, and careful scrutinizing of the photomultiplier characteristics [7]. The benefit of the thorough calibration and understanding of

pp. 2373–2376

Table 1. Summary of observations, split up into 4 bins of altitude.

Season	alt= $65-85°$	$50-65°$	$40-50°$	$15-40°$	$\sum$	$\sum$
year	[ksec]	[ksec]	[ksec]	[ksec]	[ksec]	[hrs]
1997/98	162.04	96.83	54.48	49.67	363.02	100.84
1998/99	217.84	60.82	92.15	115.72	486.52	135.15
1999/00	108.89	9.10	0.66	0.15	118.80	33.00
2000/01	129.09	39.59	17.02	2.96	188.66	52.40
2001/02	125.36	52.69	32.90	13.62	224.58	62.38

the instrument's performance is the reliable data-taking that in turn allows to combine data taken over many years with a minimum of systematics introduced by changes of the detector.

The simulations of the detector have been performed using two independent Monte-Carlo type air-shower and detector simulations [8]. Both simulations agree within 10 % on the relevant parameters (cut efficiency, rate of cosmic ray events, angular resolution, energy resolution). All detector simulations have been carried out for individual periods (one moon cycle) taking the degrading photomultiplier and optical gain into account to model the response of the detector and particularly its change with time. Additionally, whenever required, the simulations have been done with different telescope setups (3, 4, and 5-telescope setups) in case of failures of individual telescopes. The observations are taken in wobble-mode, where the telescopes point with an offset of 0.5° to the direction of the source, alternating the sign of the displacement from run to run. A summary of the observational time is given in Table 1. The listed observational times are selected for good weather conditions and instrument performance. Overall, less than 10 % of the runs have been rejected by requiring the event rate to deviate by less than 25 % from the expected value (for a given observational period and zenith angle).

The analysis technique is based upon the method first introduced for HEGRA data in [2] with the modification of applying a slightly tighter cut on the main γ/hadron separation quantity *mean scaled width*< 1.1. The *mean scaled width* is related to the width of the images scaled to the expectation for a γ-ray induced event.

For individual events at a given zenith angle, an energy estimate is calculated with a relative resolution of $\Delta E/E < 12$ % [6]. Using Monte-Carlo calculated tables of collection areas as a function of reconstructed energy for 5 discrete zenith angles a collection area for each event is calculated using interpolation in zenith angle and energy. Finally, the sum of the inverse of the collection areas is calculated for a given energy bin and using the dead-time corrected on-time, a differential flux is calculated. The background is calculated by averaging over 5

regions in the camera with the same distance to the camera center and diameter as the source region.

We have omitted to include the observations below an altitude of 40°. Further results on large zenith angle observations will be presented at the conference. The preliminary result is presented in Fig. 1. The deep exposure is sufficient to collect $\approx 10\,000$ photons used in the analysis covering 2 decades in energy. The signal in the highest energy bin centered on 39 TeV is beyond 5 σ. Inclusion of large zenith angle observations will overcome the difficulties of saturation and boost the statistics of photons up to even higher energies.

The data is well described by a pure power-law fit $dN_\gamma/dE = (2.91 \pm 0.08) \cdot 10^{-11} (E/\mathrm{TeV})^{-2.59 \pm 0.02}$ ph/(cm^2 s TeV), $\chi^2_{red}(d.o.f.) = 1.6(11)$. A functional form with a curvature term describes the data slightly better: $dN_\gamma/dE = (2.72 \pm 0.08) \cdot 10^{-11} \cdot (E/\mathrm{TeV})^{-2.43 \pm 0.05 - (0.14 \pm 0.04) \cdot \log_{10}(E/TeV)}$, $\chi^2_{red}(d.o.f.) = 0.77(10)$. A similar $\chi^2_{red}(d.o.f) = 1(7)$ is reached for a power-law with an exponential cut-off: $dN_\gamma/dE = (2.73 \pm 0.08) \cdot 10^{-11} \cdot (E/\mathrm{TeV})^{-2.43 \pm 0.05} \cdot \exp(-E/(53 \pm 38)\mathrm{TeV})$. The very slight curvature changes the photon-index from 2.43 at 1 TeV to 2.65 at 40 TeV.

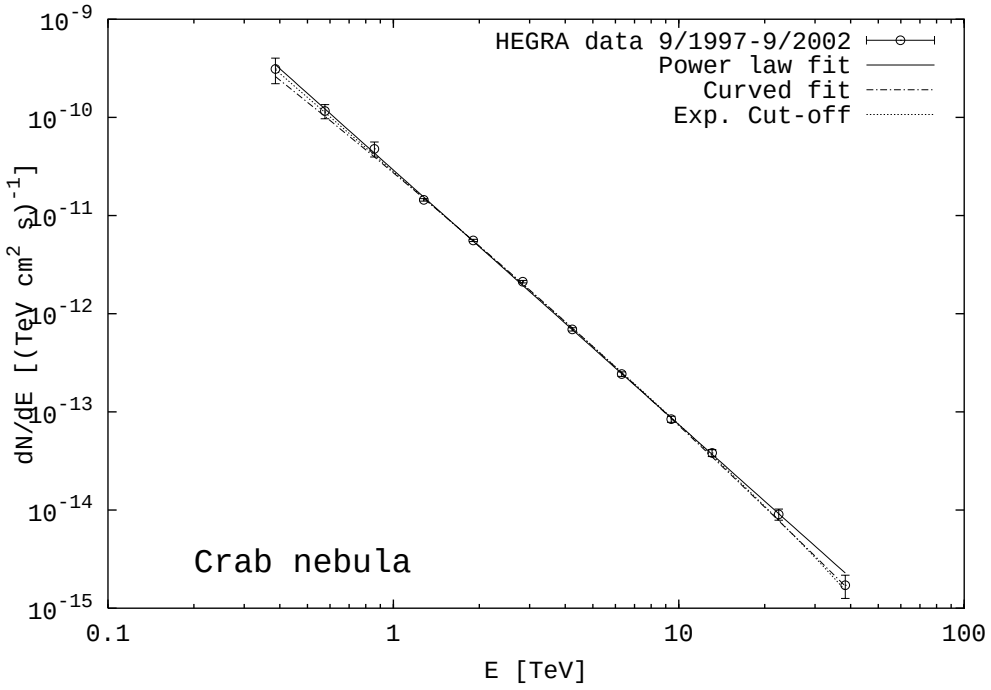

Fig. 1. The differential photon energy spectrum for the Crab nebula. The preliminary result is shown with the statistical errors only. The systematic errors are dominant below 1 TeV and above 20 TeV and are not included. Additionally, the measurement is subject to an overall uncertainty of the absolute energy scale estimated to be less than 15 %.

3. Discussion

The observations presented here cover for the first time a wide range in energies (two decades) with a single instrument. The advantage of such an observation is clearly that relative calibration uncertainties between different measurements are absent. However, there are systematic uncertainties that need to be addressed before conclusions on the physics are derived. The statistical errors of the measurement are very small (< 5 % for energies between 1 and 4 TeV) and therefore the systematic uncertainties are dominating.

The strong energy dependence of the response function of the telescopes in the threshold region is introducing uncertainties in the region below 1 TeV. Different reconstruction methods and event selections have been carried out and the variation of the response at lower energies has been studied. The conservative estimate of the systematic uncertainty below 1 TeV is a 50 % uncertainty region. This estimate is largely based upon the remaining variations in the energy spectrum below 1 TeV in different zenith angle bands and over the years of observation.

For the high energy end of the spectrum, saturation of the electronics used for digitization of the pulses is crucial. The dynamical range of the FADC electronics is limited to one order of magnitude before the individual time slices of the FADC saturate. However, using the overall pulse shape makes a larger dynamical range accessible. This introduces possible systematic effects by either over- or under-compensating. From the measured image amplitudes of cosmic ray induced events we expect these effects to be small (< 10 %). In a previous analysis [2] of large zenith angle observations where the image amplitude even for events with energies beyond 10 TeV are not saturating, no strong systematic effect was visible.

Further studies on the pulsed emission from the Crab pulsar and morphology of the γ-ray emitting region at different energies are on the way.

4. References

1. Aharonian, F.A., et al. 1999, A&A 346, 913
2. Aharonian, F.A., et al. 1999, A&A 349, 11
3. Aharonian, F.A., et al. 2000, ApJ 539, 317
4. Aharonian, F.A., et al. 2000, A&A 361, 1073
5. Aharonian, F.A., et al. 1999, A&A 346, 913
6. Hofmann, W. et al. 2000, Astrop.Physics 12, 207
7. Pühlhofer, G. et al. 2003, submitted to Astrop.Physics
8. Konopelko, A. et al. 1999, Astrop.Physics 10, 275, Bernlöhr, K. internal report, Horns, D. PhD thesis 2000